Journal of Alloys and Compounds 480 (2009) 440–448

Contents lists available at ScienceDirect

Journal of Alloys and Compounds

journal homepage: www.elsevier.com/locate/jallcom

Pressure–composition–temperature hysteresis in C14 Laves phase alloys: Part 3. Empirical formula

K. Young*, T. Ouchi, M.A. Fetcenko

Energy Conversion Devices Inc., 2983 Waterview Drive, Rochester Hills, MI 48309, USA

ARTICLE INFO

Article history:
Received 10 March 2009
Accepted 29 March 2009
Available online 23 April 2009

Keywords:
Hydrogen absorbing materials
Transition metal alloys and compounds
Metal hydride
Thermodynamic properties

ABSTRACT

In Part 1 and Part 2 of this series of papers, the pressure–concentration–temperature (PCT) isotherms hysteresis was found to be closely related to the axial ratio *a*/*c* for both simple ternary and more complicated multi-element C14 Laves phase based alloys. Furthermore, the particle pulverization rate, which is the major determining factor in the duration of metal hydride electrode cycling, was found to correlate well with PCT hysteresis. In the current Part 3, we discuss an empirical equation which was developed to predict the PCT hysteresis of battery alloys through the study of the lattice constant ratios of a series of $ZrCr_2$-based ternary alloys. The empirical formula can then be used to estimate the pulverization rate of metal hydride electrode. To fit the empirical formula, an equivalent number of outer shell electrons for some non-transition metals was calculated from the axial ratio of $ZrCr_{1.8}M_{0.2}$ ternary alloys, where M is an element from the group of Al, Si, Ga, Ge, and Sn. Other factors, such as the amount of substitution, the difference in A and B element electronegativities, atomic size, and the choice of A element, were also investigated.

1. Introduction

Metal hydride (MH) electrode disintegration due to active material pulverization is one of the key failure modes in the nickel-metal hydride (NiMH) battery [1–4]. Studies in the pulverization of various MH electrode materials were performed on AB2 [5–10], AB5 [1,11–14], A2B7 [15], V-based BCC [16], and Mg–Ni based AB materials [17]. On the newly pulverized surface, either: (1) protective layers of $La(OH)_3$ and/or $Mg(OH)_2$ formed which impeded hydrogen transportation [13,15,18–20] or (2) soluble ions such as $HZrO_3^{2-}$, $HTiO_3^{2-}$, $HMnO_2^-$, $HV_2O_5^-$ formed [6,7,21–23] which increased the self-discharge rate of the battery [5]. Both cases were due to metal oxidation in KOH electrolyte and also both caused a storage capacity reduction [24,25]. Therefore, a mathematic model or formula to predict the pulverization rate in the initial alloy design stage is highly desirable in order to extend the cycle life of the NiMH battery. However, the highly disordered nature of Laves phase based AB2 alloys makes detailed modeling very difficult. Therefore, developing an empirical formula to predict the pressure–concentration–temperature (PCT) hysteresis and pulverization rate becomes crucial to improve battery performance. Some successful examples of constructing mathematic formula based on empirical data have been previously demonstrated: MH alloy heat of formation [25–30], desorption pressure [31,32], PCT hysteresis [33], AC impedance [34], internal resistance [35], radio frequency loss [36], discharge voltage [37–40], state-of-charge [41,42], temperature [43], electrode cycle life [44], and recovery of nickel and cobalt [45] from NiMH batteries.

In Part 1 of the current series of papers, the mechanic stability of C14 Laves phase alloys was found to be strongly correlated to both the hysteresis of PCT isotherms and the ratio of lattice constants measured by X-ray diffraction analysis (XRD) [46]. A larger lattice constant ratio *a*/*c* was found to produce a smaller hysteresis between absorption and desorption isotherms resulting in less stress between the α and β phases in the hydride and less pulverization during charge/discharge cycling. In Part 2, both the PCT hysteresis and lattice constant ratio were used to correlate to the cycle performance of NiMH batteries made with MH alloys having a predominantly C14 structure. Satisfactory correlations were obtained [47]. The purpose of this Part 3 is to develop an empirical formula for the prediction of the PCT hysteresis for highly disordered, multi-element, C14-based, Laves phase alloys used as the MH active material in the electrodes of NiMH batteries. We start by studying the correlations between the lattice constant ratio *a*/*c*, average electron density (*e*/*a*), atomic size, and electronegativity difference of a series of $ZrCr_2$-based C14 alloys with various partial substitutions for Cr. Once the determining factors are identified, the empirical formula can be developed to estimate the PCT hysteresis of battery alloys.

* Corresponding author. Tel.: +1 248 293 7000; fax: +1 248 299 4520.
E-mail address: kwoyoung@yahoo.com (K. Young).

0925-8388/$ – see front matter © 2009 Elsevier B.V. All rights reserved.
doi:10.1016/j.jallcom.2009.03.194

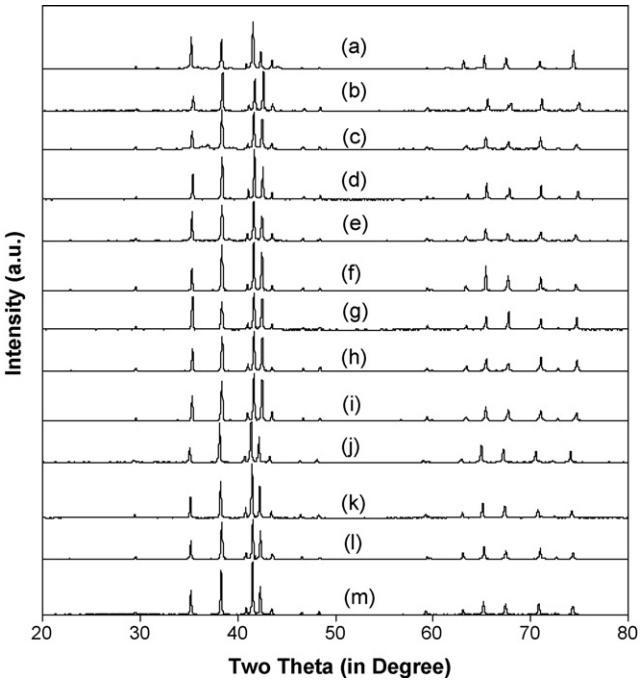

Fig. 1. XRD spectra using Cu Kα as the radiation source for alloys ZC-13 to ZC-25. All alloys in this group show a predominantly C14 structure.

2. Experimental setup

Alloys ZC-1 to ZC-12 were prepared in Part 1 of this series of papers [46]. To complete this study, an additional 13 alloys (ZC-13 to ZC-25) were fabricated by the same procedure as the previous 12. Research grade raw materials (purity > 99.9%) were weighed according to the target compositions listed in Table 1. Arc melting was performed under flowing argon with a non-consumable tungsten electrode and a water-cooled copper tray. Before each arc melt, a piece of sacrificial titanium undergoes a melting–cooling cycle a few times to reduce the residual oxygen concentration. Each 5-g ingot was re-melted and turned over periodically to ensure uniformity in the chemical composition of the sample. The chemical composition of each sample was examined by a Varian *Liberty* 100 inductively coupled plasma system. A Philips *X'Pert Pro* X-ray diffractometer was used to study the microstructure. The spectra for ZC-1 to ZC-12 can be found in Ref. [46] and those for ZC-13 to ZC-25 are shown in Fig. 1. Lattice parameters a and c were measured and listed in Table 1 together with the calculated ratio a/c, C14 unit cell volume, and Seitz radius. PCT analysis was performed with a Suzuki-Shokan multi-channel PCT system. In the PCT analysis, each sample was first activated by a 2-h thermal cycle between 300 °C and room temperature at 25 atm H_2 pressure.

3. Results and discussion

Many factors were found to influence the PCT hysteresis of hydrogen storage alloys in the scientific literature. Notable is the summary of these factors by Qian and Northwood [48]. These factors include alloy composition [49], measuring temperature [49–52], hydrogen aliquot size (H/M increment during PCT step) [53], unit cell expansion [54], particle size [55,56], number of cycles [57], and annealing process [51,58]. The contribution of measuring temperature to PCT hysteresis was described by

$$RT\ \ln\left(\frac{P_a}{P_d}\right) = B_0 + B_1T + B_2T(C - C_m) + B_3T^2(C - C_m) \quad (1)$$

where R is the ideal gas constant, T is the measuring temperature, C is the hydrogen concentration, C_m is the hydrogen concentration at the middle of isotherm plateau, and B_0, B_1, B_2, and B_3 are proportional coefficients [59]. PCT hysteresis, expressed by $RT\,ln(P_a/P_d)$ is one type of energy loss during phase transformation. Heat of hydride formation is also a type of energy and was related to the Fermi energy, lattice elastic energy, and electrostatic energy by

$$\Delta H = a_0 + a_1\left(\frac{e}{a}\right)^{2/3} + a_2d^2 + a_3(\Delta X)^2 \quad (2)$$

where a_0, a_1, a_2 and a_3 are proportion coefficients, ΔX is the average Pauling electronegativity difference among constitutional elements, d is the Goldschmidt atomic size, and e/a is the average outer number of electron density [60]. A similar formula was reported by replacing d with $\delta = \sqrt{\sum a_i\left(\frac{d_i - d_{av}}{d_{av}}\right)^2}$, where d_{av} is the average atomic radius, a_i and d_i are the atomic ratio and atomic diameter of constitutional elements in the alloy, respectively [61]. With this information in mind, we decide to explore the correlation between the lattice constant ratio (closely related to the PCT hysteresis [46,47,62,63]) and electron density, atomic size, and electronegativity in the next three sections.

3.1. Average electron density

The correlation between the lattice constant ratio in a close-packed hexagonal crystal and the number of d-band electrons for transition metals was studied by a pairwise close-packed plane interaction method [64], a moment theorem of local d-wave density of state [65], and a canonical one-electron d-eigenvalue method before [66]. The correlation between the lattice constant ratio and electron density in close-packed hexagonal phase noble metal alloys has also been studied before [67–69]. In the ζ phase, where the lattice constant ratio is around the ideal value for the close-packing of a sphere ($c/a = \sqrt{8/3} = 1.633$), the c/a vs. e/a curve resembles a right-hand half of a parabola opening downwards (Fig. 2 in Ref. [68]). However, the reason for such a correlation is not available [70].

In Fig. 3 of Part 1 of this three-part paper series, the a/c ratio of $Zr(Cr_{0.9}M_{0.1})_2$ with M = Cr, Mn, Fe, Co, Ni, Cu, and Zn was plotted against the atomic number of the substitutional element—a clear parabolic relation is found in the figure [46]. An identical correlation between a/c ratio and the atomic number of substitution element can be found on the neutron diffraction studies of $Zr(Cr_{1-x}M_x)_2$ with M = Mn, Fe, Co, Ni, Cu and $x = 0.1$ and 0.2 as reported by Soubeyroux et al. [71] (Fig. 2). The vertices of the parabolas are all near M = Co. Electron density is the first parameter explored in this study. It follows exactly the atomic number for the transition metals in this row and is a very important parameter in both calculating heat of formation (Eq. (2)) and determining the favorable Laves structure type (C14 or C15) [72,73]. Changing the average electron density by substituting B atoms with other elements can lead to changes in the crystal structure. The calculated average e/a values are listed in

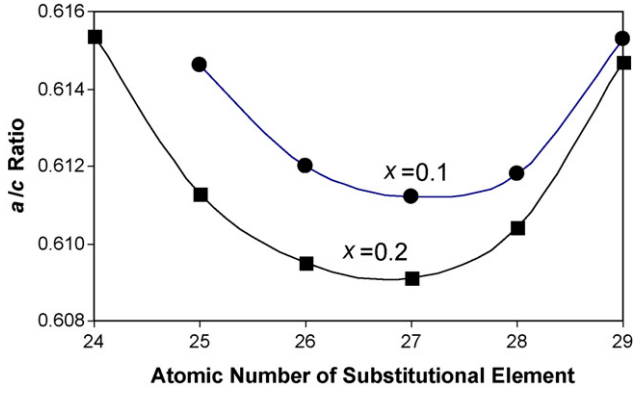

Fig. 2. Plot of ratios of a and c lattice constants measured by neutron diffraction vs. the atomic number the M on $Zr(Cr_{1-x}M_x)_2$ with M = Mn, Fe, Co, Ni, Cu and $x = 0.0$, 0.1, and 0.2. (Data from Ref. [71]).

Table 1
Summary of compositions, lattice constants from XRD analysis, axial ratio a/c, unit cell volume, Seitz radius, average B element radius [79], difference in average electronegativity between A and B elements, and average electron density calculated from the ENOSE value for each individual constituent element listed in Table 2.

	Composition	a (Å)	c (Å)	Axial ratio a/c	Unit cell volume (Å^3)	Seitz radius (Å)	Average B element radius (Å)	Difference in electronegativity	Average electron density
ZC-1	$ZrCr_2$	5.1224	8.3061	0.61670	188.7	1.958	1.4230	0.33	5.330
ZC-2	$ZrCr_{1.8}Mo_{0.2}$	5.1540	8.3394	0.61803	191.8	1.969	1.2796	0.16	5.330
ZC-3	$ZrCr_{1.8}Mn_{0.2}$	5.1074	8.3261	0.61342	188.1	1.956	1.4235	0.32	5.397
ZC-4	$ZrCr_{1.8}Ni_{0.2}$	5.0923	8.3296	0.61135	187.1	1.952	1.4184	0.36	5.598
ZC-5	$ZrCr_{1.8}Al_{0.2}$	5.1362	8.3801	0.61290	191.5	1.968	1.4390	0.32	5.624
ZC-6	$ZrCr_{1.8}Co_{0.2}$	5.0875	8.3320	0.61060	186.8	1.951	1.4192	0.35	5.531
ZC-7	$ZrCr_{1.8}V_{0.2}$	5.1258	8.3404	0.61457	189.8	1.962	1.4299	0.33	5.263
ZC-8	$ZrCr_{1.8}Cu_{0.2}$	5.1117	8.3133	0.61488	188.1	1.956	1.4220	0.35	5.665
ZC-9	$ZrCr_{1.8}Si_{0.2}$	5.1151	8.3227	0.61460	188.6	1.958	1.2796	0.16	5.666
ZC-10	$ZrCr_{1.8}Zn_{0.2}$	5.1261	8.3042	0.61729	189.0	1.959	1.4346	0.33	5.732
ZC-11	$ZrCr_{1.8}Sn_{0.2}$	5.1633	8.4381	0.61190	194.8	1.979	1.4672	0.40	5.587
ZC-12	$ZrCr_{1.8}Fe_{0.2}$	5.0945	8.3358	0.61116	187.4	1.953	1.4218	0.35	5.464
ZC-13	$ZrCr_{1.76}Ni_{0.17}Zn_{0.05}$	5.1032	8.3363	0.61217	188.0	1.956	1.4220	0.35	5.666
ZC-14	$ZrCr_{1.54}Fe_{0.42}Zn_{0.04}$	5.0718	8.3232	0.60936	185.4	1.947	1.4220	0.37	5.664
ZC-15	$ZrCr_{1.64}Fe_{0.25}Cu_{0.08}Zn_{0.02}$	5.0875	8.3391	0.61008	186.9	1.952	1.4220	0.36	5.663
ZC-16	$ZrCr_{1.30}Mn_{0.58}Ni_{0.12}$	5.0811	8.3302	0.60996	186.3	1.950	1.4220	0.31	5.665
ZC-17	$ZrCr_{1.72}Co_{0.17}Cu_{0.04}Zn_{0.04}$	5.0925	8.3299	0.61135	187.1	1.953	1.4220	0.35	5.666
ZC-18	$ZrCr_{1.76}Fe_{0.15}Ni_{0.09}$	5.0908	8.3353	0.61075	187.1	1.953	1.4204	0.35	5.531
ZC-19	$ZrCr_{1.72}Fe_{0.26}Zn_{0.02}$	5.0869	8.3318	0.61054	186.7	1.951	1.4222	0.35	5.532
ZC-20	$ZrCr_{1.63}Mn_{0.16}Fe_{0.19}Al_{0.02}$	5.0844	8.3307	0.61032	186.5	1.951	1.4365	0.35	5.531
ZC-21	$ZrCr_{1.59}Mn_{0.30}Fe_{0.09}Al_{0.02}$	5.0893	8.3344	0.61064	186.9	1.952	1.4534	0.35	5.531
ZC-22	$ZrCr_{1.8}Ga_{0.2}$	5.1244	8.3780	0.61165	190.5	1.964	1.4481	0.35	6.042
ZC-23	$ZrCr_{1.8}Ge_{0.2}$	5.1159	8.3547	0.61234	189.4	1.960	1.4564	0.37	6.073
ZC-24	$ZrCr_{1.8}V_{0.1}Co_{0.1}$	5.1083	8.3234	0.61370	188.1	1.956	1.4279	0.34	5.406
ZC-25	$ZrCr_{1.8}Al_{0.1}Ni_{0.1}$	5.1122	8.3431	0.61275	188.8	1.959	1.4321	0.34	5.619

Table 1. The measured a/c ratio was plotted against the e/a value in Fig. 3 for the first seven alloys in Table 1 and approximated by

$$\frac{a}{c} = 0.1594\left(\frac{e}{a} - 5.5223\right)^2 + 0.6112 \quad (3)$$

This parabola fit the data very well ($R^2 = 0.973$). As we apply the same parabolic model to data obtained by neutron diffraction, two equations were obtained with good fit ($R^2 = 0.987$ and 0.992 for $x = 0.1$ and 0.2, respectively, where x is the amount of substitution).

$$\frac{a}{c} = 0.2186\left(\frac{e}{a} - 5.5286\right)^2 + 0.6116 \quad (x = 0.1) \quad (4)$$

$$\frac{a}{c} = 0.0544\left(\frac{e}{a} - 5.6783\right)^2 + 0.6092 \quad (x = 0.2) \quad (5)$$

Comparing Eqs. (3) and (4), which are from the same alloy formula with different analytical tools (XRD vs. neutron diffraction), we found very similar centers and minimums and slightly different degree of openings. Interestingly enough, the leading coefficient of Eq. (4) is just four times the leading coefficient of Eq. (5), which makes the combining of two equations together relatively simple. The linear shift of the center of the parabola reflects the observation of centering on M = Co. The ideal of linear shift in the minimum comes from a series of a and c parameters reported by Bououdina et al. from $Zr(Cr_{1-x}Ni_x)_2$ with $x = 0$, 0.1, 0.2, 0.3 and 0.4 [74]. The a/c ratio as a function of x is linear for $x < 0.3$.

Therefore, we combine Eqs. (4) and (5) by introducing the substitution amount (x) as an independent variable in the following equation:

$$\begin{aligned}\frac{a}{c} &= 0.002186x^{-2}\left(\frac{e}{a} - 5.3789 - 1.497x\right)^2 + 0.6137 - 0.0245x \\ &= 0.002186\left(\frac{(e/a) - 5.3789}{x} - 1.497\right)^2 + 0.6137 - 0.0245x\end{aligned} \quad (6)$$

The calculated results from Eq. (6) are plotted against the measured a/c ratio in Fig. 4. The data fitting of a/c ratio by parabolic model was successful.

The applicable composition range ($0 < x \leq 0.2$) of Eq. (6) was verified by comparing the calculated results and measured results from

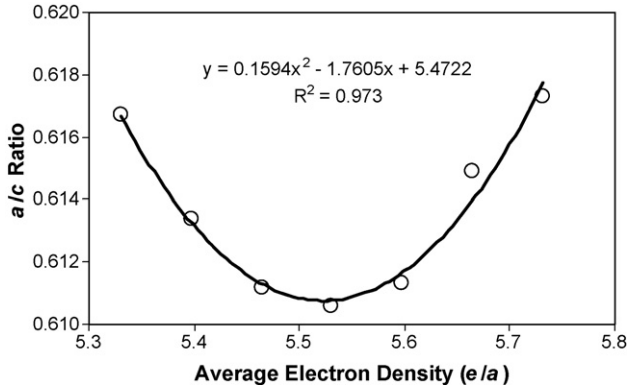

Fig. 3. Plot of ratios of a and c lattice constants measured by XRD and atomic radii vs. atomic numbers of substituents. The equation shows the best fit parabolic function with the coefficient of determination (R^2).

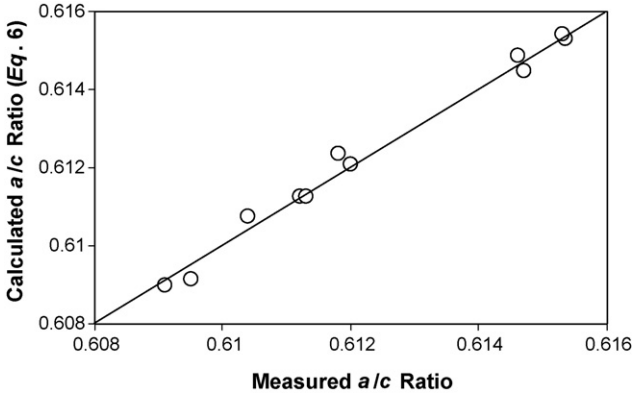

Fig. 4. Plot of the calculation result from Eq. (6) vs. the measured a/c ratio from Table 1.

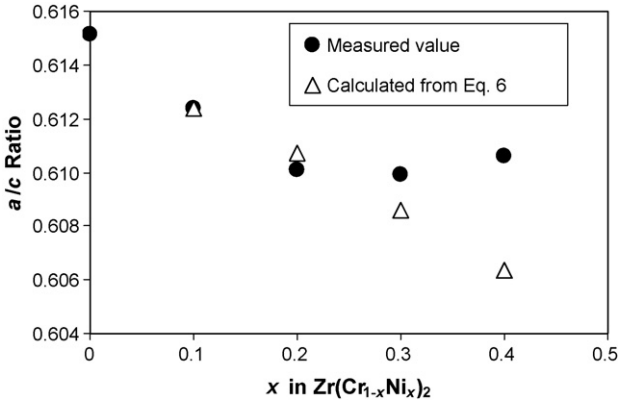

Fig. 5. Plot of the calculation result from Eq. (6) vs. the measured a/c ratio from Ref. [74].

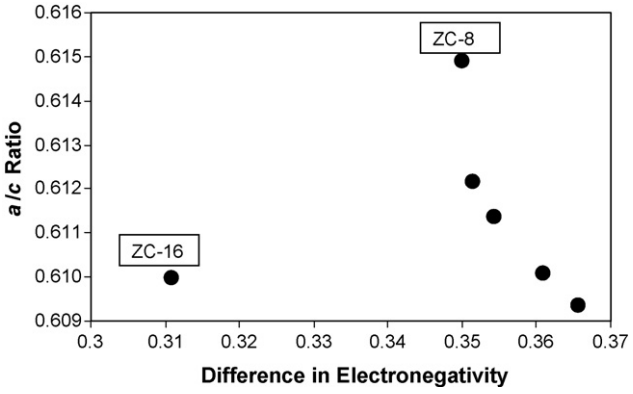

Fig. 6. Plot of the measured a/c ratio vs. the difference in A and B element average electronegativities for alloys ZC-8, ZC-13 to ZC-17 with similar atomic radius and average electron density.

Ref. [74]. The comparison is presented in Fig. 5. While the current model predicts a linear relationship between the lattice constant ratio a/c and the amount of substitution, the experimental data has a good fit up to $x = 0.2$. Additional increase in the substituted amount does not change the lattice constant ratio much. In the same paper, it was reported that as the substitution amount increases, phase segregation becomes apparent, the amount of the main structural phase decreases, and the composition of the main phase shifts away from the designed value [74]. Another possibility for the deviation from a linear dependency on the substituted amount could be that the occupancy of the substituent element in 6*h* and 2*a* sites undergoes transitions at around $x = 0.2$ [75]. This will certainly affect our model, which is based on the assumption that the site occupation change is linear and smooth. Therefore, we conclude that Eq. (6) is valid only in the range of $x < 0.3$. At a higher substitution, a more complicated multi-phase situation including changes in substitution site preferences cannot be modeled by the empirical formula derived from a single phase case.

3.2. Average difference in electronegativity

Lattice constants and lattice energy are affected by the difference in average electronegativities of the A and B elements as defined by $\Delta X = \sum_i b_i X_i - \sum_j a_j X_j$, where b_i and a_j are the atomic ratios for the B element j and the A element i. This can be seen from the last term in Eq. (2), which is the electrostatic energy from the Pauling electronegativity difference. In general, a larger difference in electronegativity contributes to a higher tendency of uneven electron probability distribution and shortens the lattice constant [76]. Whether this shortening is isotropic or non-isotropic has not previously been reported. In this section, we design five alloys (ZC-13 to ZC-17) to duplicate the average atomic radius and electron density of alloy ZC-8 with the intention to study the influence of difference in electronegativities to lattice constant ratio. The results are listed in Table 1 and plotted in Fig. 6. Except for alloys with the highest (ZC-16) and the lowest (ZC-8) levels of substitution, the a/c ratios of the alloys show a good linear dependency on the difference in electronegativity. As the electronegativity difference increases, the lattice constant a decreases monotonically while c fluctuates and the a/c ratio decreases linearly within a small substitution range. The substitution amount is known to play an important role in determining the a/c ratio from Eq. (6), and its influence is larger than that of the difference in electronegativity. Therefore, the difference in electronegativities was excluded as an independent variable in further formula construction.

3.3. Average atomic radius

In Fig. 3 of Part 1 of this three-part series, the a/c ratio is plotted against the atomic number of the substitute element and also against the atomic radius of the substitute element [46]. The general trends of these two curves are similar with a small shift in the parabolic minima. It is important to determine whether the correlation relates to the atomic number (which has been taken into account by consideration of the average electron density) or the atomic size of the constituent element. The prediction of heat of formation in Eq. (2) includes a term from the contribution of a lattice parameter ($a_2 d^2$). Lattice parameters are certainly strongly influenced by the atomic radius of the constituent element. Therefore, it is possible that atomic radius contributes to PCT hysteresis, which is another form of energy. Instead of the average atomic radius, which can be altered by the different distribution of valence electron [77], the Seitz radius, defined by $r_S = \sqrt[3]{\frac{4\times\text{volume of unit cell}}{3\pi\times\text{number of atomin unit cell}}}$, is closer to the real lattice parameter in the crystal and was previously used to correlate with PCT hysteresis [78]. The Seitz radii of all ternary alloys $ZrCr_{1.8}X_{0.2}$ with the same substitution level ($x = 0.2$) in this study are plotted against the a/c ratios in Fig. 7. While the general trend of a larger a/c ratio corresponds to a larger Seitz radius for transition metal substitution, the correspondence for non-transition metal substitution is in the opposite direction.

In order to investigate the contribution from electron density and electronegativity difference, four alloys (ZC-18 to ZC-21) were designed to duplicate the electronegativity and electron density of alloy ZC-6 with the intention to study the influence of atomic

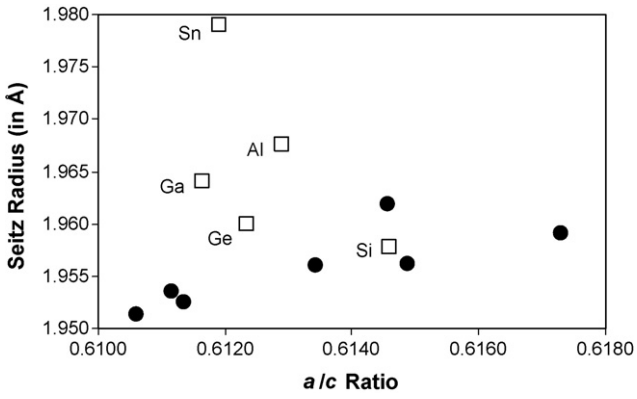

Fig. 7. Plot of the Seitz radius of M vs. the a/c ratio for the ternary alloys $ZrCr_{1.8}M_{0.2}$.

Table 2
Numbers of outside shell electrons and the calculated equivalent numbers of outside shell electrons (ENOSE) for selective elements.

Element	Al	Si	Ti	V	Cr	Mn	Fe	Co	Ni	Cu	Zn	Ga	Ge	Zr	Mo	Sn
# of shell e⁻	3	4	4	5	6	7	8	9	10	11	12	3	4	4	6	4
ENOSE	10.4	11	4	5	6	7	8	9	10	11	12	9.6	10.1	4	6	9.8

radius in lattice constant ratio. We used atomic radii derived from Laves phase crystal [79]. The results are listed in Table 1 and plotted in Fig. 8. Lattice parameters a and c and their ratio show very little variance with different radii of the substitute elements. As a result of this observation, the average atomic radius was excluded as an independent parameter in further empirical formula development. This decision is in agreement with Dwight's argument: When electron transfer takes place, atoms will change size and move toward ideal ratio [80]. Therefore, the final lattice constant may not have a direct relationship to the atomic radius of the constituent elements.

3.4. Equivalent number of outer shell electrons for other B elements

In order to generalize the formula in Eq. (6) to include the non-transition metals commonly used in NiMH battery applications, a new equivalent number of outer shell electrons (ENOSE) must be calculated and assigned to these elements. Cockayne and Raynor first demonstrated this approach by using the lattice constant ratio to find the equivalent valence for some transitional metals [81]. Eq. (3) was rearranged to solve for e/a and the measured values of a/c ratios from five alloys (ZC-5 (Al), ZC-9 (Si), ZC-22 (Ga), ZC-23 (Ge), and ZC-11(Sn)) were inserted into the equation. The sign of the solution for the quadratic equation was chosen based on results from other ternary alloys such as ZC-25 and alloys as in Ref. [82]. The calculated ENOSE for the elements Al, Si, Ga, Ge, and Sn are 10.39, 11.02, 9.63, 10.1 and 9.83, respectively. Although these numbers are much higher than the real number of outer shell electrons, they are consistent with the fact that in the determination of the electron density of noble metal or aluminum alloys with transition metals, it is often practical to exclude the d-band electrons from transition metallic elements, such as Fe, Co, Ni [83]. Therefore, the difference in the number of valance electron between Al and Fe, Co, and Ni used in the calculation will be around 1, which is close to the difference in the ENOSE value developed in this study. There is an average increase of 0.5 ENOSE in moving from Column III to Column IV elements (the fact that the increase is <1 electron is interesting). As the row number of the element increases, the ENOSE decreases monotonically. The corresponding implications for physics may be worthy of further investigation.

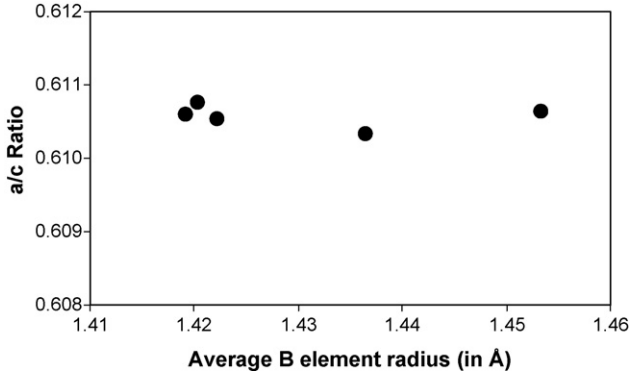

Fig. 8. Plot of the measured a/c ratio vs. the average atomic radius of B element in alloys ZC-6, ZC-18 to ZC-21 with similar electronegativity difference and average electron density.

Due to its low electron density, the ternary alloy with vanadium substitution, ZC-7, turns out to be structurally predominantly C15 phase and is not suitable for calculating the ENOSE value for vanadium [46]. ZC-24 was made to calculate the ENOSE value for vanadium. The XRD spectrum of this alloy shows it to be structurally predominantly C14 phase (Fig. 1(l)) and when the a/c ratio was used in Eq. (3), the calculated e/a was 4.78, which is very close to the real number of outer shell electron (5). Therefore, 5 is used as the ENOSE value for vanadium in the following calculation of average electron density. As a result of this study, the ENOSE for some commonly used B element modifiers are listed in Table 2.

3.5. Contribution from A elements

The development of an empirical formula for predicting the a/c ratio has so far concentrated on B element modifiers. The two main A elements, Ti and Zr, have the same number of outer shell electrons, and should have no effect to the formula based on average electron density. A series of $Ti_xZr_{33.5-x}(VNiCrMnCoAl)_{66.5}$ C14 alloys with varying Ti and Zr contents have been studied before [84]. Lattice constants and their ratios obtained from XRD analysis together with the PCT hysteresis measured at 1.0 wt.% storage capacity are listed in Table 3. These alloys have a relatively low plateau pressure at 30 °C and PCT data are not available at 0.5 wt.% storage capacity for most of the alloys (see Fig. 5b in Ref. [84]). Thus, 1.0 wt.% was chosen instead. As seen in Table 3, the a/c ratio first increases and then remains constant with increasing Ti-content. The change in the slope is related to the sudden change in entropy and enthalpy of this series of alloys (Fig. 6 in Ref. [84]). The lattice constant ratio changes with Ti-content in a narrow range and is difficult to fit to a mathematic formula. The correlation between Ti-content and PCT hysteresis is also hard to establish. Therefore, the contribution from different Ti/Zr content was ruled out from our empirical formula by keeping the ENOSE value the same as their real number of outer shell electron (4 for both Ti and Zr).

3.6. Empirical formula for battery alloys

The commonly used C14 Laves phase based hydrogen storage alloys in NiMH battery application are more complicated than the

Table 3
Lattice constants, axial ratio, and PCT hysteresis measured at 1.0 wt.% storage capacity for a series of $Ti_xZr_{33.5-x}$ $(VNiCrMnCoAl)_{66.5}$ C14 alloys.

Alloy #	Ti-content	a (in Å)	c (in Å)	a/c	Hys at 30 °C
B1	16.5	4.964	8.120	0.6113	0.22
B2	17.0	4.958	8.100	0.6121	0.20
B3	17.5	4.955	8.092	0.6123	0.54
B4	18.0	4.955	8.081	0.6132	0.45
B5	18.5	4.958	8.073	0.6141	0.15
B6	19.0	4.947	8.073	0.6128	0.11
B7	19.5	4.946	8.071	0.6128	0.10
B8	20.0	4.943	8.068	0.6127	0.15
B9	20.5	4.942	8.068	0.6125	0.18

Table 4
Lattice constants, axial ratio, and PCT hysteresis measured at 1.0 wt.% storage capacity for a series of $TiZrV_xNi_{38.5-x}CrMnCoAl$ C14 alloys.

Alloy #	V-content	a (in Å)	c (in Å)	a/c	Hys at 30 °C
D1	10.0	4.939	8.059	0.6129	6.559
D2	11.0	4.945	8.067	0.6130	6.509
D3	12.0	4.948	8.076	0.6127	6.459
D4	13.0	4.950	8.085	0.6122	6.409
D5	14.0	4.953	8.088	0.6124	6.359
D6	15.0	4.957	8.086	0.6130	6.309
D7	16.0	4.962	8.095	0.6130	6.259
D8	17.0	4.974	8.126	0.6121	6.209
D9	18.0	4.977	8.137	0.6117	6.159

simple $ZrCr_2$-based alloys discussed above. The multi-phase nature of these alloys causes a very high degree of disorder and therefore they are difficult to mathematically model [85]. We have previously reported on our study of a series of $TiZrV_xNi_{38.5-x}CrMnCoAl$ AB2 alloys with nickel being partially replaced by vanadium [86]. Since vanadium and nickel are the B elements with the lowest and highest ENODE values, it makes this series of alloys the best candidate for studying the influence of average electron density on some properties of interest. The lattice constants calculated from XRD analysis together with the PCT hysteresis of these alloys are listed in Table 4 and both parameters are plotted against the average electron density based on the ENOSE value of constituent element of the alloys in Fig. 9. Considering the wide range of average electron densities, the changes in a/c ratio are very small when compared with the data in Fig. 3. The changes in a/c ratio are small and hard to fit with a reasonable mathematic function. On the other hand, PCT hysteresis monotonically decreases with increasing average electron density. Therefore, it is concluded that for highly disordered battery alloys, PCT hysteresis is more easily modeled as a function of average electron density than lattice constant ratio while both parameters can be correlated to the pulverization rate of the alloy (which is important in the battery application).

A group of 112 MH electrode alloys were prepared by induction melting. Batch sizes ranged from 2 to 500 kg. The designed chemical compositions of these alloys are listed in Table 5 in atomic percentages. The final compositions of these alloys were verified by both X-ray fluorescence and inductively coupled plasma methods to be within 1% of target values. The average electron density for each alloy was calculated based on the ENOSE value of the individual constituents and listed in Table 2. PCT hysteresis (Hys) value, which is defined as the natural logarithm of the ratio between absorption equilibrium pressure and desorption equilibrium pressure at 0.5 wt.% of the hydrogen storage, is also listed in the same table.

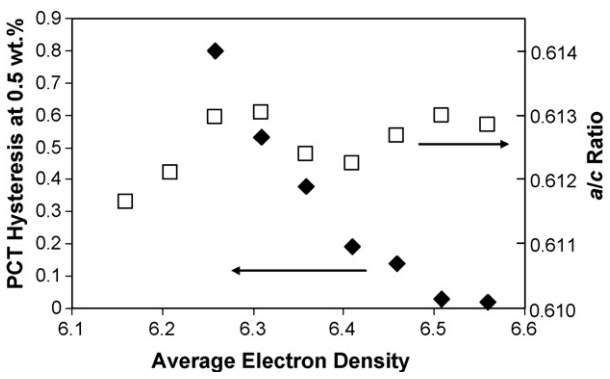

Fig. 9. Plot of both PCT hysteresis and a/c ratio as a function of the average electron density of a series of $TiZrV_xNi_{38.5-x}CrMnCoAl$ alloys from Ref. [86].

Choosing 0.5 wt.% is arbitrary and consistent with our prior publications [87–89]. The reciprocal of Hys (i.e. 1/Hys) was plotted against the average electron density because the Hys vs. lattice constant ratio plot suggested a reciprocal relationship (Fig. 9 in Ref. [46]). From Fig. 9, a clear parabolic relationship can be established similar to Fig. 3 with shift in the minimum from 5.5 to 6.5. The empirical formula for estimating PCT hysteresis from the electron density value for battery alloys is:

$$\frac{1}{\text{Hys}} = 46\left(\frac{e}{a}\right)^2 - 603\left(\frac{e}{a}\right) + 1978 \tag{7}$$

where e/a is the average electron density of the constituent elements in the alloy formula calculated by

$$\frac{e}{a} = \sum_i a_i \text{ENOSE}_i \tag{8}$$

where a_i and ECOSE_i are, respectively, the atomic ratio and equivalent number of outer shell electron as listed in Table 2 for constituent element i. To determine if there is any impact of Ti-content to PCT hysteresis, these alloys can be further categorized by their Ti-content (as shown by the different symbols in Fig. 10). Both Ti and Zr have the same ENOSE value, but their contributions to PCT hysteresis cannot be distinguished using Eq. (7). Alloys with similar Ti-content formed different sections of the parabola of Fig. 10, but no specific distribution can be found within the individual groups. Alloys with lower Ti-content must have higher Zr content to maintain AB2 stoichiometry. The combination of high-Zr with low-Ti increases the metal–hydrogen bond strength and therefore, the vanadium content must be reduced in order to maintain the metal–hydrogen bond strength. The decrease in vanadium (ENOSE = 5) happens mainly at the expense of nickel (ENOSE = 10) and therefore the average electron density is on the high side when the Ti-content is small. This explains the distribution of groups with different levels of Ti-content in Fig. 10. Those alloys with lower Ti-content appear more on the right hand side of the figure.

As the study in Section 3.1 indicates, the substitution amount (variable x) is very important in the equation developed for simple $ZrCr_2$-based alloys (Eq. (6)). The data in Table 5 was re-grouped according to Ni content to study the influence of substitution amount to the PCT hysteresis. The results are shown in Fig. 11. Again, the distribution in average electron density is not uniform. Also, there is a direct correlation between Ni content and average electron density due to its very high ENOSE value. In each subgroup, no special correlation was found; therefore, the amount of substitution has no direct impact to the hysteresis of battery alloys even

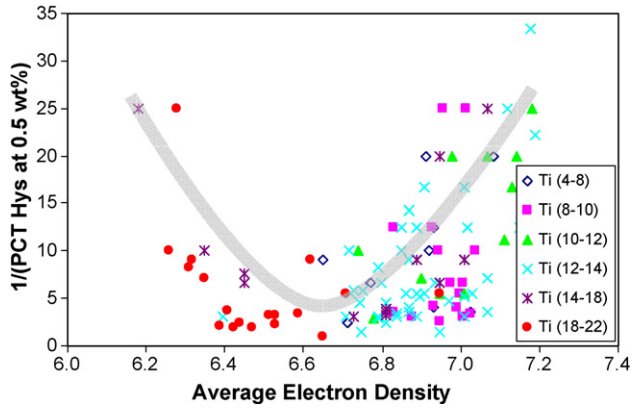

Fig. 10. Plot of the reciprocal of PCT hysteresis measured at 0.5 wt.% storage capacity vs. the average electron density of alloys in Table 5. Data points were grouped by their Ti-contents.

Table 5
Compilation of negative electrode alloys composition, calculated average electron density, and PCT hysteresis at 0.5 wt.% storage capacity.

Alloy #	Ti	Zr	V	Ni	Cr	Mn	Co	Al	Fe	Sn	Mo	*e*/*a*	Hys
1	4.0	28.5	0.0	23.2	14.6	23.4	5.6	0.7	0.0	0.0	0.0	6.71	0.40
2	5.0	30.7	5.0	37.6	5.0	16.0	0.0	0.4	0.0	0.3	0.0	6.93	0.08
3	6.0	27.0	8.0	29.3	10.0	19.0	0.0	0.4	0.0	0.3	0.0	6.65	0.11
4	6.0	29.7	5.0	37.6	5.0	16.0	0.0	0.4	0.0	0.3	0.0	6.93	0.25
5	7.0	27.0	8.0	34.3	10.0	13.0	0.0	0.4	0.0	0.3	0.0	6.77	0.15
6	7.0	28.6	5.0	37.6	5.0	16.5	0.0	0.0	0.0	0.3	0.0	6.92	0.10
7	7.0	29.0	5.0	37.6	5.0	16.0	0.0	0.4	0.0	0.0	0.0	6.91	0.05
8	7.0	29.1	4.0	40.2	4.0	15.0	0.0	0.4	0.0	0.3	0.0	7.03	0.28
9	7.9	26.2	4.5	37.3	4.8	15.5	0.0	3.5	0.0	0.3	0.0	7.09	0.05
10	8.0	27.7	5.0	37.6	5.0	16.0	0.0	0.4	0.0	0.3	0.0	6.93	0.24
11	8.0	28.1	4.0	35.2	4.0	20.0	0.0	0.4	0.0	0.3	0.0	6.88	0.32
12	8.0	28.1	4.0	40.2	4.0	15.0	0.0	0.4	0.0	0.3	0.0	7.03	0.29
13	8.0	29.0	0.0	29.0	8.0	10.0	15.5	0.5	0.0	0.0	0.0	7.01	0.15
14	8.6	26.0	4.7	37.2	5.6	17.5	0.0	0.4	0.0	0.0	0.0	6.94	0.10
15	8.7	28.1	4.5	34.4	5.3	17.1	1.5	0.4	0.0	0.0	0.0	6.83	0.28
16	8.7	28.1	4.5	35.9	5.3	17.5	0.0	0.0	0.0	0.0	0.0	6.83	0.08
17	8.8	25.8	5.0	37.8	3.7	16.2	0.5	0.0	1.4	0.8	0.0	7.01	0.33
18	8.8	26.0	5.0	37.8	3.7	16.2	0.5	0.0	1.7	0.3	0.0	6.99	0.25
19	8.8	26.0	5.0	37.8	3.7	16.2	0.0	0.5	1.7	0.3	0.0	7.00	0.18
20	9.0	26.6	5.0	38.0	5.0	15.6	0.0	0.4	0.0	0.4	0.0	6.95	0.38
21	9.0	26.6	5.0	38.0	5.0	15.4	0.0	0.6	0.0	0.4	0.0	6.95	0.04
22	9.0	26.7	5.0	38.0	5.0	16.0	0.0	0.0	0.0	0.3	0.0	6.93	0.08
23	9.0	27.0	4.0	40.2	4.0	15.5	0.0	0.0	0.0	0.3	0.0	7.01	0.04
24	9.2	25.1	5.0	37.2	3.5	15.4	1.3	0.5	2.0	0.8	0.0	7.04	0.10
25	9.2	26.4	5.0	37.2	3.5	15.4	0.0	0.5	2.0	0.8	0.0	6.97	0.15
26	10.0	23.5	10.0	36.2	5.5	9.1	5.0	0.4	0.0	0.3	0.0	6.95	0.18
27	10.0	23.5	10.0	38.2	5.5	7.1	5.0	0.4	0.0	0.3	0.0	7.01	0.18
28	10.0	23.5	10.0	40.2	5.5	5.1	5.0	0.4	0.0	0.3	0.0	7.07	0.05
29	10.0	24.7	8.0	34.0	10.0	12.6	0.0	0.4	0.0	0.3	0.0	6.74	0.10
30	10.0	27.0	0.0	30.0	8.0	15.0	5.0	5.0	0.0	0.0	0.0	6.98	0.05
31	10.0	27.0	0.0	35.0	8.0	10.0	5.0	5.0	0.0	0.0	0.0	7.13	0.06
32	10.0	27.0	0.0	35.0	3.0	15.0	5.0	5.0	0.0	0.0	0.0	7.18	0.04
33	10.0	27.0	0.0	40.0	5.0	13.0	5.0	0.0	0.0	0.0	0.0	7.14	0.05
34	10.5	23.0	9.0	33.2	8.5	13.6	1.5	0.4	0.0	0.3	0.0	6.78	0.34
35	10.5	23.0	9.0	36.2	5.5	13.6	1.5	0.4	0.0	0.3	0.0	6.90	0.14
36	11.0	26.0	0.0	40.0	8.0	10.0	5.0	0.0	0.0	0.0	0.0	7.11	0.09
37	12.0	21.5	10.0	28.7	8.5	13.6	3.5	1.9	0.0	0.3	0.0	6.71	0.10
38	12.0	21.5	10.0	31.7	8.5	13.6	1.5	0.4	0.5	0.3	0.0	6.72	0.18
39	12.0	21.5	10.0	32.2	8.5	13.6	1.5	0.4	0.0	0.3	0.0	6.73	0.17
40	12.0	21.5	10.0	32.2	6.5	15.6	1.5	0.4	0.0	0.3	0.0	6.75	0.65
41	12.0	21.5	10.0	32.2	6.5	13.6	3.5	0.4	0.0	0.3	0.0	6.79	0.35
42	12.0	21.5	10.0	32.2	8.5	10.1	5.0	0.4	0.0	0.3	0.0	6.80	0.15
43	12.0	21.5	10.0	32.2	8.5	10.1	1.5	3.9	0.0	0.3	0.0	6.85	0.08
44	12.0	21.5	10.0	32.2	7.5	8.1	8.0	0.4	0.0	0.3	0.0	6.87	0.11
45	12.0	21.5	10.0	34.1	8.5	13.6	0.0	0.0	0.0	0.3	0.0	6.74	0.22
46	12.0	21.5	10.0	34.2	8.5	11.6	1.5	0.4	0.0	0.3	0.0	6.79	0.33
47	12.0	21.5	10.0	34.2	6.5	13.6	1.5	0.4	0.0	0.3	0.0	6.81	0.28
48	12.0	21.5	10.0	36.2	14.5	3.6	1.5	0.4	0.0	0.3	0.0	6.79	0.12
49	12.0	21.5	10.0	36.2	12.5	5.6	1.5	0.4	0.0	0.3	0.0	6.81	0.41
50	12.0	21.5	10.0	36.2	8.5	9.6	1.5	0.4	0.0	0.3	0.0	6.85	0.10
51	12.0	21.5	10.0	36.2	7.5	9.6	1.5	0.4	1.0	0.3	0.0	6.87	0.28
52	12.0	21.5	10.0	36.2	6.5	11.6	1.5	0.4	0.0	0.3	0.0	6.87	0.25
53	12.0	21.5	10.0	36.2	4.5	11.6	1.5	0.4	0.0	0.3	2.0	6.87	0.07
54	12.0	21.5	10.0	36.2	4.5	13.6	1.5	0.4	0.0	0.3	0.0	6.89	0.08
55	12.0	21.5	10.0	36.2	6.5	9.6	1.5	0.4	2.0	0.3	0.0	6.89	0.18
56	12.0	21.5	10.0	36.2	5.5	9.6	1.5	0.4	3.0	0.3	0.0	6.91	0.06
57	12.0	21.5	10.0	36.2	2.5	15.6	1.5	0.4	0.0	0.3	0.0	6.91	0.18
58	12.0	21.5	10.0	36.2	3.4	13.6	1.5	1.5	0.0	0.3	0.0	6.94	0.15
59	12.0	21.5	10.0	36.2	5.5	9.1	5.0	0.4	0.0	0.3	0.0	6.95	0.71
60	12.0	21.5	10.0	36.2	5.5	6.1	8.0	0.4	0.0	0.3	0.0	7.01	0.33
61	12.0	21.5	10.0	36.2	0.0	9.6	1.5	0.4	8.5	0.3	0.0	7.02	0.08
62	12.0	21.5	10.0	36.3	10.0	8.0	1.5	0.4	0.0	0.3	0.0	6.84	0.33
63	12.0	21.5	10.0	37.2	7.7	9.0	1.9	0.4	0.0	0.3	0.0	6.89	0.19
64	12.0	21.5	10.0	38.1	8.5	9.6	0.0	0.0	0.0	0.3	0.0	6.86	0.18
65	12.0	21.5	10.0	38.2	10.5	5.6	1.5	0.4	0.0	0.3	0.0	6.89	0.32
66	12.0	21.5	10.0	38.2	5.5	7.1	5.0	0.4	0.0	0.3	0.0	7.01	0.06
67	12.0	21.5	10.0	39.7	1.0	13.6	1.5	0.4	0.0	0.3	0.0	7.03	0.18
68	12.0	21.5	10.0	39.7	5.5	5.1	5.0	0.4	0.0	0.8	0.0	7.07	0.28
69	12.0	21.5	10.0	40.2	8.5	5.6	1.5	0.4	0.0	0.3	0.0	6.97	0.21
70	12.0	21.5	10.0	40.2	5.5	5.1	5.0	0.4	0.0	0.3	0.0	7.07	0.14
71	12.0	21.5	10.0	40.2	3.5	4.1	8.0	0.4	0.0	0.3	0.0	7.15	0.08
72	12.0	21.5	10.0	43.2	3.5	4.1	5.0	0.4	0.0	0.3	0.0	7.18	0.03
73	12.0	21.5	10.0	44.2	5.5	4.6	1.5	0.4	0.0	0.3	0.0	7.12	0.04
74	12.0	21.5	10.0	46.7	3.5	4.1	1.5	0.4	0.0	0.3	0.0	7.21	0.10
75	12.0	21.5	12.0	36.2	10.0	8.0	0.0	0.0	0.0	0.3	0.0	6.75	0.17
76	12.0	21.5	14.0	36.2	4.5	9.6	1.5	0.4	0.0	0.3	0.0	6.81	0.22

Table 5 (*Continued*)

Alloy #	Ti	Zr	V	Ni	Cr	Mn	Co	Al	Fe	Sn	Mo	*e*/*a*	Hys
77	12.0	25.0	0.0	37.0	8.0	8.0	5.0	5.0	0.0	0.0	0.0	7.19	0.05
78	12.5	22.0	13.0	26.0	9.0	17.5	0.0	0.0	0.0	0.0	0.0	6.40	0.33
79	13.0	20.5	10.0	36.3	10.0	8.0	1.5	0.4	0.0	0.3	0.0	6.84	0.29
80	13.0	20.5	10.0	40.2	4.5	9.6	1.5	0.4	0.0	0.3	0.0	7.01	0.19
81	13.5	20.0	11.0	32.2	8.5	12.6	1.5	0.4	0.0	0.3	0.0	6.71	0.33
82	14.0	19.5	10.0	32.2	8.5	13.6	1.5	0.4	0.0	0.3	0.0	6.73	0.33
83	14.0	19.5	10.0	36.2	4.5	13.6	1.5	0.4	0.0	0.3	0.0	6.89	0.11
84	14.0	19.5	10.0	36.2	5.5	9.1	5.0	0.4	0.0	0.3	0.0	6.95	0.05
85	14.0	19.5	10.0	38.2	5.5	7.1	5.0	0.4	0.0	0.3	0.0	7.01	0.11
86	14.0	19.5	10.0	40.2	5.5	5.1	5.0	0.4	0.0	0.3	0.0	7.07	0.04
87	14.0	19.5	12.0	26.2	10.0	18.0	0.0	0.0	0.0	0.3	0.0	6.45	0.15
88	14.0	19.5	14.0	36.2	4.5	9.6	1.5	0.4	0.0	0.3	0.0	6.81	0.31
89	15.0	18.5	14.0	36.2	4.5	9.6	1.5	0.4	0.0	0.3	0.0	6.81	0.26
90	16.0	17.5	12.0	26.2	10.0	18.0	0.0	0.0	0.0	0.3	0.0	6.45	0.13
91	16.0	17.5	14.0	24.2	10.0	18.0	0.0	0.0	0.0	0.3	0.0	6.35	0.10
92	16.0	17.5	14.0	36.2	4.5	9.6	1.5	0.4	0.0	0.3	0.0	6.81	0.28
93	16.5	17.0	13.0	19.5	14.0	20.0	0.0	0.0	0.0	0.0	0.0	6.18	0.04
94	17.0	16.5	10.0	36.2	5.5	9.1	5.0	0.4	0.0	0.3	0.0	6.95	0.15
95	18.0	15.5	14.0	21.2	10.0	20.5	0.0	0.5	0.0	0.3	0.0	6.28	0.04
96	18.0	15.5	14.0	21.2	8.5	20.6	1.5	0.4	0.0	0.3	0.0	6.32	0.11
97	18.0	15.5	14.0	22.2	10.0	18.0	0.0	0.0	2.0	0.3	0.0	6.31	0.12
98	18.0	15.5	14.0	24.2	10.0	18.0	0.0	0.0	0.0	0.3	0.0	6.35	0.14
99	18.0	15.5	14.0	24.2	10.5	15.6	1.5	0.4	0.0	0.3	0.0	6.39	0.47
100	18.0	15.5	14.0	24.2	8.5	17.6	1.5	0.4	0.0	0.3	0.0	6.41	0.27
101	18.0	15.5	14.0	26.2	8.5	15.6	1.5	0.4	0.0	0.3	0.0	6.47	0.51
102	18.0	15.5	14.0	27.2	10.0	15.0	0.0	0.0	0.0	0.3	0.0	6.44	0.41
103	18.0	15.5	14.0	28.2	8.5	13.6	1.5	0.4	0.0	0.3	0.0	6.53	0.45
104	18.0	15.5	14.0	30.2	10.0	12.0	0.0	0.0	0.0	0.3	0.0	6.53	0.31
105	18.0	15.5	14.0	30.2	8.5	11.6	1.5	0.4	0.0	0.3	0.0	6.59	0.29
106	18.0	15.5	14.0	32.2	8.5	9.6	1.5	0.4	0.0	0.3	0.0	6.65	0.98
107	20.0	13.5	14.0	21.2	10.0	21.0	0.0	0.0	0.0	0.3	0.0	6.26	0.10
108	21.0	12.5	14.0	31.7	10.0	8.6	1.5	0.4	0.0	0.3	0.0	6.62	0.11
109	21.0	12.5	14.0	34.7	10.0	5.6	1.5	0.4	0.0	0.3	0.0	6.71	0.18
110	21.0	12.8	14.0	27.2	10.0	15.0	0.0	0.0	0.0	0.0	0.0	6.42	0.52
111	21.0	12.8	14.0	30.2	10.0	12.0	0.0	0.0	0.0	0.0	0.0	6.51	0.31
112	22.0	11.5	10.0	36.2	5.5	9.1	5.0	0.4	0.0	0.3	0.0	6.95	0.18

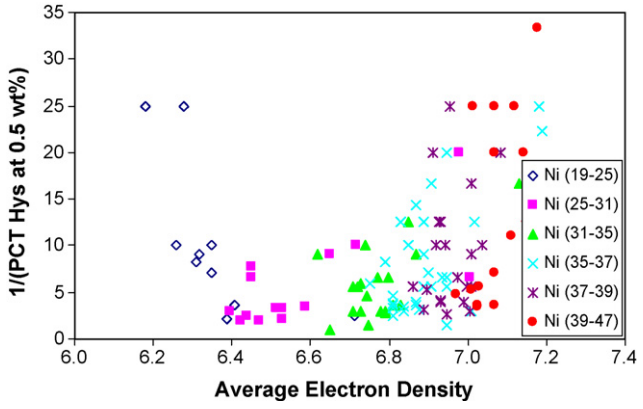

Fig. 11. Plot of the reciprocal of PCT hysteresis measured at 0.5 wt.% storage capacity vs. the average electron density of alloys in Table 5. Data points were grouped by their Ni-contents.

though the amount of substitution is important to the simple alloy (due to its contribution to the degree of disorder).

4. Conclusions

An empirical formula was developed to predict the PCT hysteresis for the C14 Laves phase based hydrogen storage alloys used as negative electrode active material in NiMH batteries. The single factor, average electron density, was chosen from the study of the lattice constant ratio of a series of $ZrCr_2$-based C14 alloys. Both electronegativity and atomic radius were ruled out as independent variables for estimating lattice constant ratio. For the non-transition metals commonly used as B element modifier, an ENOSE value was assigned according to the *a*/*c* ratio in $ZrCr_{1.8}M_{0.2}$. The reciprocal of PCT hysteresis has a parabolic dependence on the average electron density of the alloy. Long cycle life AB2 alloys suitable for NiMH battery application will have an average electron density either: (1) smaller than 6.4 or (2) greater than 6.9.

References

[1] J.J.G. Willems, Philips J. Res. 39 (1984) 10.
[2] R.C. Ambrosio, E.A. Ticianelli, J. Power Sources 110 (2002) 73.
[3] D. Chartouni, F. Meli, A. Züttel, K. Gross, L. Schlapbach, J. Alloys Compd. 241 (1996) 160.
[4] S. Vivet, M. Latroche, Y. Chabre, J.-M. Joubert, B. Knosp, A. Percheron-Guégan, Phys. B: Condens. Matter 362 (2005) 199.
[5] J.S. Yu, S.M. Lee, K. Cho, J.Y. Lee, J. Electrochem. Soc. 147 (2000) 2013.
[6] X.-P. Gao, Y.-M. Sun, E. Toyoda, E. Higuchi, T. Nakagima, S. Suda, Electrochim. Acta 45 (2000) 3099.
[7] Y. Xu, C. Chen, X. Wang, Y. Lei, Q. Wang, J. Alloys Compd. 337 (2002) 214.
[8] H. Pan, Y. Zhu, M. Gao, Y. Liu, R. Li, Y. Lei, Q. Wang, J. Alloys Compd. 364 (2004) 271.
[9] Y. Zhu, H. Pan, M. Gao, Y. Liu, R. Li, Y. Lei, Q. Wang, Int. J. Hydrogen Energy 29 (2004) 313.
[10] J. Wang, H. Pan, R. Li, K. Zhong, M. Gao, Int. J. Hydrogen Energy 32 (2007) 3381.
[11] T. Sakai, K. Oguro, H. Miyamura, N. Kuriyama, A. Kato, H. Ishikawa, C. Iwakura, J. Less-Common Met. 161 (1990) 193.
[12] P.H.L. Notten, R.E.F. Einerhand, J.L.C. Daams, J. Alloys Compd. 231 (1995) 604.
[13] W. Liu, Y. Lei, D. Sun, J. Wu, Q. Wang, J. Power Sources 58 (1996) 243.
[14] F. Laurencelle, Z. Dehouche, J. Goyette, J. Alloys Compd. 424 (2006) 266.
[15] Y. Liu, H. Pan, M. Gao, Y. Lei, Q. Wang, J. Electrochem. Soc. 152 (2005) A1089.
[16] M. Tsukahara, K. Takahashi, A. Isomura, T. Sakai, J. Alloys Compd. 287 (1999) 215.
[17] C. Rongeat, L. Roué, J. Alloys Compd. 404–406 (2005) 679.
[18] P. Leblanc, C. Jordy, B. Knosp, P. Blanchard, J. Electrochem. Soc. 145 (1998) 860.
[19] Y. Osumi, Suiso-kyuzo-goukin no Syurui to Sono, new ed., Agune Technology Center, Tokyo, Japan, 1999, p. 478.
[20] S. Ruggeri, L. Roué, J. Huot, R. Schulz, L. Aymard, J.-M. Tarascon, J. Power Sources 112 (2002) 527.
[21] M. Pourbaix, Atlas of Electrochemical Equilibria in Aqueous Solution, 77027, National Association of Corrosion Engineers, Houston, TX, 1974, p. 290.

[22] B. Reichman, W.C. Mays, K. Young, M.A. Fetcenko, S.R. Ovshinsky, Electrochem. Soc. Proc. 98–15 (1998) 111.
[23] B.H. Liu, Z.P. Li, Y. Matsuyama, R. Kitani, S. Suda, J. Alloys Compd. 296 (2000) 201.
[24] A.H. Boonstra, T.N.M. Bernards, G.J.M. Lippits, J. Less-Common Met. 159 (1990) 327.
[25] A. Züttle, F. Meli, L. Schlapbach, J. Alloys Compd. 203 (1994) 235.
[26] P.C.P. Bouten, A.R. Miedema, J. Less-Common Met. 71 (1980) 147.
[27] A.L. Shilov, M.E. Kost, N.T. Kuznetsov, J. Less-Common Met. 105 (1985) 221.
[28] A. Percheron-Guégan, C. Lartigue, J.C. Achard, J. Less-Common Met. 109 (1985) 287.
[29] A.L. Shilov, M.E. Kost, N.T. Kuznetsov, J. Less-Common Met. 128 (1987) 1.
[30] K. Hong, J. Alloys Compd. 321 (2001) 307.
[31] G. Busch, L. Schlabach, A. Seiler, in: A.F. Andresen, J.A. Maeland (Eds.), Hydrides for Energy Storage, Pergamon Press, Oxford, 1978, p. 293.
[32] X. Wang, C. Wang, C. Chen, Q. Wang, J. Alloys 420 (2006) 107.
[33] H. Nakamura, Y. Nakamura, S. Fujitani, I. Younezu, J. Alloys Compd. 252 (1997) 83.
[34] E. Kuhn, C. Forgez, P. Lagonotte, G. Friedrich, J. Power Sources 158 (2006) 1490.
[35] J. Larminie, J. Lowry, Electrical Vehicle Technology Explained, John Wiley & Sons, Inc., New York, 2003, p. 38.
[36] E. Hoene, S. Guttowski, R. Saikly, W. John, H. Reichl, IEEE Electromagnetic Compatibility Society: IEEE International Symposium on Electromagnetic Compatibility EMC 2003 IEEE Service Center, Vol. 1, Piscataway, NJ, 2003, p. 425.
[37] B. Wu, M. Mohammed, D. Brigham, R. Elder, R.E. White, J. Power Sources 101 (2001) 149.
[38] M. Verbrugge, E. Tate, J. Power Sources 126 (2004) 236.
[39] E. Wilhelm, M.W. Fowler, R.A. Fraser, M.B. Stevens, Proceeding of PHEV2007, November 1–2, Winnipeg, Manitoba, Canada, 2007.
[40] M. Thele, O. Bohlen, D.U. Saue, E. Karden, J. Power Sources 175 (2008) 635.
[41] Y.M. Podrazhansky, Y.Y. Kusharskiy, US Patent 6,281,683 (2001).
[42] M.W. Verbrugge, E.D. Tate, Jr., S.D. Sarbacker, B.J. Koch, US Patent 6,359,419 (2002).
[43] A.A. Pesaran, J. Power Sources 110 (2002) 377.
[44] P.H.L. Notten, R.E.F. Einerhand, J.L.C. Daams, J. Alloys Compd. 210 (1994) 221.
[45] N. Tzanetakis, K. Scott, J. Chem. Technol. Biotechnol. 79 (2004) 919.
[46] K. Young, T. Ouchi, M.A. Fetcenko, J. Alloys Compd. (2008), doi:10.1016/j.jallcom.2008.12.113.
[47] K. Young, T. Ouchi, W. Mays, B. Reichman, M.A. Fetcenko, J. Alloys Compd. (2008), doi:10.1016/j.jallcom.2008.12.115.
[48] S. Qian, D.O. Northwood, Int. J. Hydrogen Energy 13 (1988) 25.
[49] V.K. Sinka, W.E. Wallace, J. Less-Common Met. 91 (1983) 239.
[50] A.Y. Esayed, D.O. Northwood, Int. J. Hydrogen Energy 16 (1991) 687.
[51] M.N. Mungole, R. Balasubramaniam, K.N. Rai, Int. J. Hydrogen Energy 20 (1995) 151.
[52] S.N. Klyamkin, N.S. Zakharkina, A.A. Tsikhotskaya, J. Alloys Compd. 398 (2005) 145.
[53] S. Qian, D.O. Northwood, Int. J. Hydrogen Energy 17 (1992) 631.
[54] M.T. Hagström, S.N. Klyamkin, P.D. Lund, J. Alloys Compd. 293–295 (1999) 67.
[55] J.-M. Park, Y.-G. Kim, J.-Y. Lee, J. Alloys Compd. 198 (1993) L19.
[56] E. Rabkin, V.M. Skripnyuk, Scripta Mater. 49 (2003) 477.
[57] A. Esayes, D.O. Northwood, Int. J. Hydrogen Energy 19 (1994) 591.
[58] S.N. Klyamkin, N.S. Zakharkina, J. Alloys Compd. 361 (2003) 200.
[59] S. Fang, Z. Zhou, J. Zhang, M. Yao, F. Feng, D.O. Northwood, Int. J. Hydrogen Energy 25 (2000) 143.
[60] S. Fang, Z. Zhou, J. Zhang, M. Yao, F. Feng, D.O. Northwood, J. Alloys Compd. 293–295 (1999) 10.
[61] Z. Shuang, L. Qin, C. Ning, M. Li, Y. Wen, J. Alloys Compd. 287 (1999) 57.
[62] Y. Osumi, H. Suzuki, A. Kato, K. Oguro, S. Kawai, M. Kaneko, J. Less-Common Met. 89 (1983) 287.
[63] Y. Osumi, Suiso-kyuzo-goukin no Syurui to Sono, new ed., Agune Technology Center, Tokyo, Japan, 1999, p. 218.
[64] C.H. Hodges, Acta Metall. 15 (1967) 1787.
[65] F. Ducastelle, F. Cyrot-Lackmann, J. Phys. Chem. Solids 32 (1971) 285.
[66] J.X. Zheng-Johansson, O. Eriksson, B. Johansson, Phys. Rev. B 59 (1999) 6131.
[67] T.B. Massalski, H.W. King, Prog. Mater. Sci. 10 (1961) 1.
[68] T.B. Massalski, J. Phys. Badium 23 (1962) 647.
[69] T.B. Massalski, H.W. King, Acta Met. 10 (1962) 1171.
[70] G.S. Rohrer, Structure and Bonding in Crystalline Materials, Cambridge University Press, Cambridge, UK, 2001, p. 426.
[71] J.L. Soubeyroux, M. Bououdina, D. Fruchart, L. Pontonnier, J. Alloys Compd. 219 (1995) 48.
[72] F. Laves, H. Witte, Metallwirt 15 (1936) 840.
[73] O. Bernauer, J. Töpler, D. Noréus, R. Hempelmann, D. Richter, Int. J. Hydrogen Energy 14 (1989) 187.
[74] M. Bououdina, J.L. Soubeyroux, D. Fruchart, Int. J. Hydrogen Energy 22 (1997) 329.
[75] X. Yan, A. Grytsic, P. Rogl, H. Schmidt, G. Giester, Comp. Coupling Phase Diagrams Thermochem. (2008), doi:10.1016/j.calphad.2008.07.006.
[76] S. Wakao, Hydrogen Storage Alloys (Material properties and applications), New Technology Series 6, Power Co., Tokyo, Japan, 1993, p. 75.
[77] F. Stein, M. Palm, G. Sauthoff, Intermetallics 12 (2004) 713.
[78] T. Kodama, J. Alloys Compd. 278 (1998) 194.
[79] Nihon Kinzoku Gakkai, Hi Kagaku Ryouronteki Kinzoku Kagobutu, Maruzen, Tokyo, 1975, p.296.
[80] A.E. Dwight, Trans. ASM 53 (1961) 479.
[81] B. Cockayne, G.V. Raynor, Proceedings of the Royal Society of London Series A Mathematical and Physical Sciences 261, 1961, p. 175.
[82] A. Drašner, Ž. Blažina, J. Alloys Compd. 199 (1993) 101.
[83] P. Haasen, Physical Metallurgy, third ed., Cambridge University Press, Cambridge, UK, 1995, p. 139.
[84] K. Young, T. Ouchi, F. Li, M.A. Fetcenko, J. Alloys Compd. 464 (2008) 238.
[85] S.R. Ovshinsky, M.A. Fetcenko, J. Ross, Science 260 (1993) 176.
[86] K. Young, T. Ouchi, F. Li, M.A. Fetcenko, J. Alloys Compd. 468 (2009) 482.
[87] K. Young, M.A. Fetcenko, T. Ouchi, F. Li, J. Koch, J. Alloys Compd. 469 (2009) 406.
[88] K. Young, T. Ouchi, M.A. Fetcenko, J. Alloys Compd. (2008), doi:10.1016/j.jallcom.2008.09.146.
[89] K. Young, T. Ouchi, J. Koch, M.A. Fetcenko, J. Alloys Compd. (2008), doi:10.1016/j.jallcom.2008.10.102.